Robust vetoes for gravitational-wave burst triggers using known instrumental couplings

P Ajith†, M Hewitson†, J R Smith† and K A Strain†‡

† Max-Planck-Institut für Gravitationsphysik (Albert-Einstein-Institut) und Universität Hannover, Callinstr. 38, 30167 Hannover, Germany
‡ Department of Physics and Astronomy, University of Glasgow, Glasgow, G12 8QQ, United Kingdom

E-mail: `Ajith.Parameswaran@aei.mpg.de`

Abstract.
  The search for signatures of transient, unmodelled gravitational-wave (GW) bursts in the data of ground-based interferometric detectors typically uses 'excess-power' search methods. One of the most challenging problems in the burst-data-analysis is to distinguish between actual GW bursts and spurious noise transients that trigger the detection algorithms. In this paper, we present a unique and robust strategy to 'veto' the instrumental glitches. This method makes use of the phenomenological understanding of the coupling of different detector sub-systems to the main detector output. The main idea behind this method is that the noise at the detector output (channel H) can be projected into two orthogonal directions in the Fourier space – along, and orthogonal to, the direction in which the noise in an instrumental channel X would couple into H. If a noise transient in the detector output originates from channel X, it leaves the statistics of the noise-component of H orthogonal to X unchanged, which can be verified by a statistical hypothesis testing. This strategy is demonstrated by doing software injections in simulated Gaussian noise. We also formulate a less-rigorous, but computationally inexpensive alternative to the above method. Here, the parameters of the triggers in channel X are compared to the parameters of the triggers in channel H to see whether a trigger in channel H can be 'explained' by a trigger in channel X and the measured transfer function.

1. Introduction

A world-wide network of gravitational-wave (GW) detectors consisting of ground-based interferometers [1, 2, 3, 4] and resonant-bars [5, 6, 7] has now started looking for signatures of GWs expected to be coming from astrophysical and cosmological sources. Among the most promising astrophysical sources of GWs for these ground-based detectors are the transient, unmodelled astrophysical phenomena like core-collapse supernovae, Gamma-ray bursts and black hole/neutron star mergers. Although, in recent years, numerical relativity has made a tremendous progress in predicting the gravitational waveforms from compact binary mergers and gravitational collapses (see, for e.g., [8] for some recent work), these predictions are not yet robust enough so as to allow the data-analysts to use techniques like matched filtering, which relies on the accurate models of waveforms. Most of the algorithms currently used in burst-searches are time-frequency detection algorithms which look for short-lived excitations of power in time-frequency maps constructed from the time-series data [9, 10, 11]. Such

detection algorithms implemented in the data analysis pipelines are usually called event trigger generators (ETGs).

Since current interferometric detectors are highly complex instruments, the detector output will contain a large number of spurious noise transients which trigger the ETGs. One of the main challenges in the burst-data-analysis is to distinguish these instrumental 'glitches' from actual GW bursts. One way of approaching the problem is to use more than one detector (mostly located at different parts of the world) and look for coincident burst signals in these data streams. While coincident instrumental bursts in multiple detectors are highly improbable, long data-taking runs (typically several months long) with multiple detectors can produce a large number of random coincidences. All of the detector groups are thus developing various techniques to 'veto' the spurious instrumental bursts at the detector site itself in order to reduce the list of candidate coincident triggers (see [12, 13, 14] for some recent work in this direction).

In this paper we present a robust veto strategy which makes use of a phenomenological understanding of the coupling of various detector sub-systems with the main detector output. This provides us the possibility of vetoing the triggers with a very high confidence. Although this method was developed for the GEO 600 [3] detector, this can be applied to the data from any interferometric GW detector.

The main idea behind this method is that the noise measured at the detector output can be decomposed into two orthogonal components. If the physical coupling between a sub-system X and the detector output is measured, this information can be used to *transfer*, or *map*, the noise in X to the detector output, and hence the component of H orthogonal to the 'mapped' X can also be calculated. If a noise transient originating from the sub-system X appears in the detector output, it leaves the statistics of the noise in the direction orthogonal to the mapped X unchanged. In Sections 2 and 3 we formulate and demonstrate a strategy to veto such noise transients using the *transfer function* from X to H. In Section 4, we develop an alternative veto strategy using the parameters of the burst triggers estimated by the ETG.

2. Vetoes using known instrumental couplings

Let $x(t)$ and $h(t)$ denote the time-series data measured at the input and output of a linear, time-invariant system. The input and output of the system are related by the *transfer function* $T_{\mathrm{XH}}(s)$ of the system, defined as [15]

$$T_{\mathrm{XH}}(s) = \frac{H(s)}{X(s)},\tag{1}$$

where $H(s)$ and $X(s)$ represent the Laplace transforms of $x(t)$ and $h(t)$, respectively, and the complex variable s represents a point in the Laplace space. Although the transfer function $T_{\mathrm{XH}}(s)$ is formally defined in the Laplace space, for the purpose of this paper, it is easier to work in the Fourier domain. If $\tilde{X}(f)$ and $\tilde{H}(f)$ are the Fourier transforms of $x(t)$ and $h(t)$, respectively, the equivalent relation in the Fourier domain is given by

$$T_{\mathrm{XH}}(f) = \frac{\tilde{H}(f)}{\tilde{X}(f)},\tag{2}$$

or,

$$T_{\mathrm{XH}}(f) = \frac{P_{\mathrm{XH}}}{P_{\mathrm{XX}}},\tag{3}$$

where P_{XH} is the cross-power spectral density of $x(t)$ and $h(t)$, and P_{XX} is the power spectral density of $x(t)$. In the formal language of signal processing, $T_{\mathrm{XH}}(f)$ is described by the *frequency response* (magnitude of $T_{\mathrm{XH}}(f)$) and *phase-shift* (phase of $T_{\mathrm{XH}}(f)$). But we will conveniently think of $T_{\mathrm{XH}}(f)$ and $T_{\mathrm{XH}}(s)$ as two different representations of the transfer function.

We will refer to the measurement points for time-series data within the detector as 'channels' and assume that they are continuously recorded. Let $x(t)$ and $h(t)$ denote the time-series data in channel X (which, presumably records the noise from a detector sub-system) and channel H (the main detector output), respectively. The transfer function from X to H can be measured by injecting some noise in X and measuring $\tilde{X}(f)$ and $\tilde{H}(f)$ simultaneously [16]. This is done in such a way that the injected noise from X completely dominates channel H, and the contributions from other noise sources are negligible. The measured transfer function represents our phenomenological understanding of the physical coupling of a detector sub-system to the main detector output. If we assume that the coupling of noise between channel X and H is linear and the transfer function is time-invariant, the Fourier transform of noise measured in channel X at any time can be *transferred* to channel H, by

$$\tilde{X}'(f) = T_{\mathrm{XH}}(f)\,\tilde{X}(f). \tag{4}$$

$\tilde{X}(f)$ and $\tilde{H}(f)$ can be thought of as components of the vectors $\tilde{\mathbf{X}}$ and $\tilde{\mathbf{H}}$, defined in two different infinite-dimensional Hilbert spaces spanned by the Fourier basis functions. In that sense, Eq.(4) is equivalent to mapping $\tilde{\mathbf{X}}$ into the space of $\tilde{\mathbf{H}}$. Then, the component of $\tilde{\mathbf{H}}$ that is orthogonal to $\tilde{\mathbf{X}}'$ can be found by a Gram-Schmidt orthogonalization [17]

$$\tilde{\boldsymbol{\delta}} = \tilde{\mathbf{H}} - \mathrm{proj}_{\tilde{\mathbf{X}}'}\tilde{\mathbf{H}}, \tag{5}$$

where we define the projection operator by

$$\mathrm{proj}_{\tilde{\mathbf{u}}}\tilde{\mathbf{v}} = \frac{\langle \tilde{\mathbf{v}}, \tilde{\mathbf{u}} \rangle}{\langle \tilde{\mathbf{u}}, \tilde{\mathbf{u}} \rangle}\,\tilde{\mathbf{u}}. \tag{6}$$

In the above expression $\langle \tilde{\mathbf{v}}, \tilde{\mathbf{u}} \rangle$ denotes the inner product between the vectors $\tilde{\mathbf{v}}$ and $\tilde{\mathbf{u}}$:

$$\langle \tilde{\mathbf{v}}, \tilde{\mathbf{u}} \rangle = 2 \int_0^\infty \tilde{v}(f)\,\tilde{u}(f)^*\,\mathrm{d}f. \tag{7}$$

All of the continuous quantities like $\tilde{H}(f)$ and $\tilde{X}(f)$ can be recast in terms of their discrete counterparts like $\tilde{H}_k$ and $\tilde{X}_k$, where the index k represents the kth frequency bin of the discrete Fourier transform (DFT). Now $\tilde{\mathbf{H}}$ and $\tilde{\mathbf{X}}$ can be thought of as vectors defined in two N-dimensional Hilbert spaces, where N is the number of data samples used to compute the DFTs.

The noise in different channels is generated by different random processes and has specific statistical and spectral properties. If a non-stationarity (e.g., a glitch) originates in channel X, it will change the statistical properties of that segment of data in channel X, and hence, in channel H. But the statistical properties of $\tilde{\boldsymbol{\delta}}$ constructed from this segment will remain unaffected. On the other hand, if the non-stationarity does *not* originate in X, it *will* change the statistical properties of $\tilde{\boldsymbol{\delta}}$ constructed from this segment. This can be verified by a statistical hypothesis testing. If $\tilde{\boldsymbol{\delta}}$ constructed from the segment of data containing the non-stationarity is statistically similar to that constructed from the neighboring segments, this means that the non-stationarity originates in an instrumental sub-system (channel X) and we veto the trigger. If this

is not true, this means that the non-stationarity does *not* originate in channel X, and we keep the trigger. This exercise can be repeated with all the known noise sources (all the measured channels that are known to couple to the detector output).

2.1. Test statistic

If the components of $\tilde{\mathbf{H}}$ are generated by zero-mean Gaussian processes, the real and imaginary parts of $\tilde{\delta}_k$ in each frequency bin will be distributed according to a Gaussian distribution of mean zero and variance σ_k^2. Following [9], we compute the 'excess-power' statistic from $\tilde{\boldsymbol{\delta}}$:

$$\epsilon = \sum_{k=m}^{m+M} P_k , \quad P_k = \frac{|\tilde{\delta}_k|^2}{\sigma_k^2}. \tag{8}$$

It can be shown that ϵ will follow a χ^2 distribution of $2M$ degrees of freedom in the case of a non-windowed DFT. But in the case of a windowed DFT, P_k are not *independent* χ^2 variables, and hence ϵ will *not* follow a χ^2 distribution [18]. But to a very good approximation, ϵ will follow a Gamma distribution with scale parameter α and shape parameter β. These parameters are related to the mean and variance of the distribution of ϵ by

$$\alpha = \left(\frac{\mu_\epsilon}{\sigma_\epsilon}\right)^2, \quad \beta = \frac{\sigma_\epsilon^2}{\mu_\epsilon}. \tag{9}$$

In order to estimate the parameters of the Gamma distribution, we generate a population of ϵ from stationary data surrounding the burst (using the same DFT-length and bandwidth). From that population, μ_ϵ and σ_ϵ^2 can be estimated, and hence α and β.

If the computed ϵ (from the segment of data containing the burst) is less than a threshold, we veto the trigger. The threshold τ giving a rejection probability of ψ can be found by

$$\psi = \int_0^\tau \Gamma(x; \alpha, \beta) \, \mathrm{d}x, \tag{10}$$

where $\Gamma(x; \alpha, \beta)$ is the probability density of the Gamma distribution with parameters α and β.

3. Implementation

Two sets of burst triggers are generated by running an ETG on channels X and H. We take a set of triggers that are coincident in channels X and H, allowing a liberal time-window for coincidence. The data is divided into N number of segments, each of length L. The test statistic, ϵ, is computed from the segment of data containing the burst. It is well-known that the maximum signal-to-noise ratio (SNR) for the 'excess power' statistic is achieved when the time-frequency volume used to compute the statistic is equal to the actual time-frequency volume of the signal [9]. Since the duration and bandwidth of the burst is estimated by the ETG itself, this information is used to decide on the length (L) of the data-segment used to compute $\tilde{\delta}_k$ and the bandwidth over which the integration is carried out in Eq.(8). Consequently, the frequency resolution of the DFT used in the analysis is in general different for each trigger, and hence, so are the dimension of the vectors $\tilde{\mathbf{H}}$ and $\tilde{\mathbf{X}}$. It is then
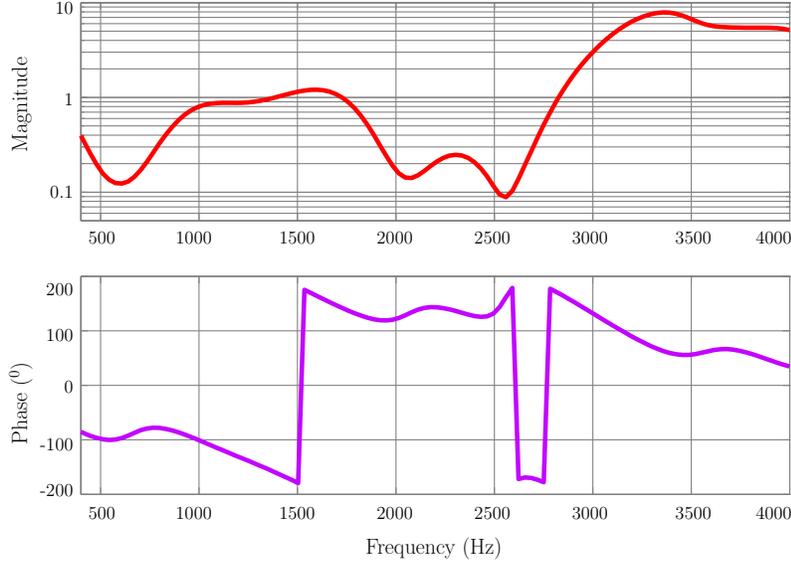
Figure 1. Transfer function $T_{\mathrm{XH}}(f)$ from channel X to channel H used for the simulations.

required that the discrete transfer function vector should also have the same dimension. So we store a high-resolution transfer function and interpolate it to the required frequency resolution. It was found that the analysis can be sensitive to the errors in the interpolation, since the interpolation can smear out the detailed features in the transfer function. Since, the lower the frequency resolution the higher are the errors, we set up a minimum frequency resolution of 16 Hz for the analysis. In order to achieve this, the minimum length of the data segment used to compute the DFT is set to be $1/16$ s $\simeq 60$ ms.

The parameters of the Gamma distribution are estimated from segments of data neighboring the one containing the burst, but excluding that segment. The trigger is vetoed if $\epsilon \leq \tau$, where the threshold τ giving a particular rejection probability ψ is calculated using Eq.(10).

3.1. Software injections

Let us define some terminology. The rejection probability is the *probability* of a trigger originating from channel X being vetoed using the method described above. The veto efficiency is the fraction of such triggers that are *actually* vetoed. In order to demonstrate that the obtained veto efficiency is in good agreement with the rejection probability, we simulate a population of bursts in channel X and H such that these are consistent with the transfer function from channel X to H. We then try to veto these triggers after choosing a specific rejection probability. If all of our assumptions are valid, the fraction of vetoed triggers among this population should be equal to the rejection probability.

We generate a data stream of Gaussian white-noise and 'inject' Gaussian-modulated sinusoidal waveforms in to it; this forms our channel X. This data stream is filtered using a time-domain filter and some extra noise is added to it. This constitutes
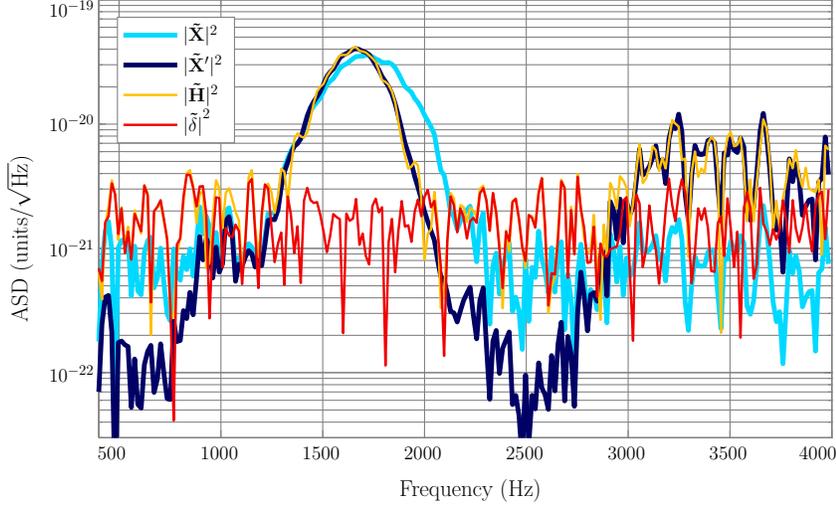
Figure 2. Amplitude spectral densities of $\tilde{\mathbf{X}}$, $\tilde{\mathbf{X}}'$, $\tilde{\mathbf{H}}$ and $\tilde{\boldsymbol{\delta}}$ in the presence of a sine-Gaussian injection. It can be seen that $\tilde{\boldsymbol{\delta}}$ contains no trace of the injected signal. The injected sine-Gaussian has a central frequency of 1715 Hz and SNR of 140 in channel X.

our channel H (the 'extra' noise being the component of $\tilde{\mathbf{H}}$ orthogonal to $\tilde{\mathbf{X}}'$). The frequency response of the filter is the transfer function from X to H. The transfer function used in this simulation is shown in Figure 1, which is quite similar to one particular transfer function measured in GEO 600. The injected sine-Gaussians are of the form:

$$s(t) = s_{\text{rss}} \left(\frac{2f_0^2}{\pi} \right)^{1/4} \sin\left[2\pi f_0(t - t_0)\right] \exp\left[-(t - t_0)^2/\tau^2\right], \qquad (11)$$

where f_0 is the central frequency of the waveforms and t_0 is the time corresponding to the peak amplitude. We setup the envelope width as $\tau = 2/f_0$. The corresponding quality factor is $Q \equiv \sqrt{2}\pi f_0 \tau = 8.9$ and bandwidth is $\Delta f = f_0/Q \simeq 0.1 f_0$. The quantity s_{rss} is the root-sum-squared (RSS) amplitude:

$$\left[\int_{-\infty}^{\infty} s^2(t)\,\mathrm{d}t \right]^{1/2} = s_{\text{rss}}. \qquad (12)$$

The s_{rss} is varied so that the SNR ‡ of the injections ranges from $\simeq 6$ to $\simeq 500$ in channel X, and the central frequency is randomly chosen from the interval (432 Hz, 3008Hz).

As an illustration, the amplitude spectral densities of $\tilde{\mathbf{X}}$ (data vector in channel X), $\tilde{\mathbf{X}}'$ (data vector in X, mapped to H), $\tilde{\mathbf{H}}$ (data vector in channel H) and $\tilde{\boldsymbol{\delta}}$ (component of $\tilde{\mathbf{H}}$ that is orthogonal to $\tilde{\mathbf{X}}'$) in the presence of a particular sine-Gaussian injection are shown in Figure 2. The injected sine-Gaussian has a central frequency of 1715 Hz and SNR of 140 in channel X. As expected, $\tilde{\boldsymbol{\delta}}$ contains no trace of the injected signal.

‡ The SNR, ρ, of a burst trigger is defined by $\rho^2 \equiv 2 \int \left(|\tilde{s}(f)|^2 / |\tilde{n}(f)|^2 \right) \mathrm{d}f$ where $\tilde{s}(f)$ and $\tilde{n}(f)$ represent the Fourier transforms of the signal and the underlying noise, respectively, and the integration is carried out over the bandwidth (positive frequencies) of the burst waveform.
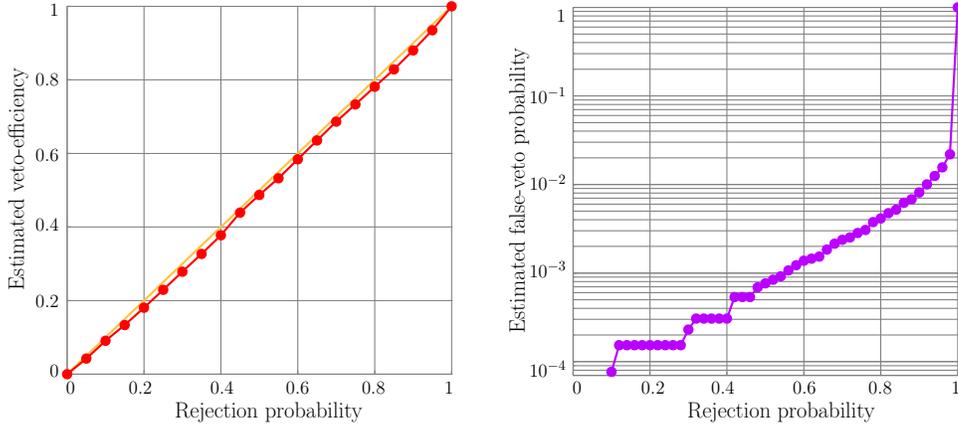
Figure 3. [*Left*]: Estimated veto efficiency plotted against the rejection probability. [*Right*]: Estimated false-veto probability plotted against the rejection probability.

The fraction of vetoed events among the injections is plotted against the rejection probability corresponding to the chosen threshold in Figure 3 (left). It can be seen that the obtained veto efficiency is in very good agreement with the chosen rejection probability.

There is a non-zero probability for an instrumental burst which does not originate in X, or a true GW burst, to be vetoed using this method. But, since the probability densities of neither GW bursts nor instrumental bursts are known *a priori*, there is no rigorous method for estimating this 'false-rejection'/'false-veto' probability. As a plausible estimation, we inject two populations of sine-Gaussian waveforms with random parameters into two data streams of white-noise (so that the waveforms in channel X and H are inconsistent with the transfer function from X to H). We then try to veto these triggers using the transfer function from X to H. The estimated 'false-veto fraction' is plotted against the chosen rejection probability in Figure 3 (right). This suggests that veto efficiencies of ≥ 92 % can be achieved with a false-veto probability of $\leq 1\%$.

4. An alternative method: 'trigger mapping'

Although the above described method is rigorous and makes use of the complete information contained in the data, the method can be computationally expensive because it involves reprocessing of the time series data from the two channels. It may be noted that the whole data stream is processed by the ETG in the first place and a condensed form of the information about the burst waveform is stored (which is often known as 'metadata'). In this section, we develop a strategy to veto the spurious triggers in channel H by comparing them with the set of triggers in channel X, making use of the transfer function from X to H as well as the information extracted by the ETG. Although this method is not as rigorous as the previous one, the advantage is that this does not require the reprocessing of time-series data and hence is computationally inexpensive.

Let $\{\mathbf{E_X}\}$ and $\{\mathbf{E_H}\}$ denote the set of burst triggers in channel X and channel H,
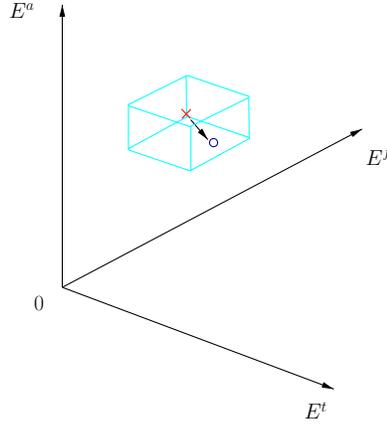
Figure 4. A schematic diagram of the parameter space of burst triggers. The cross represents a trigger in channel H and the circle represents a trigger in channel X, mapped to channel H. A distance vector $\mathbf{w}$ is drawn from one point to another. The consistency volume chosen to veto the trigger is also shown.

respectively. Let us assume that each event, $\mathbf{E}$, is parametrized by its central frequency E^f, amplitude E^a and time-of-occurrence E^t. It is useful to think of $\mathbf{E}$ as a point in a three-dimensional parameter space with coordinates (E^a, E^f, E^t). Using the transfer function from X to H, we can predict how a certain event $\mathbf{E}_X$ would appear in H. In other words, we map the event $\mathbf{E}_X$ to the space of $\mathbf{E}_H$, making use of the transfer function from X to H. In order to veto an event $\mathbf{E}_H$ in channel H, we check whether any of the 'mapped' $\mathbf{E}_X$ triggers are consistent with $\mathbf{E}_H$ in time-of-occurrence, central frequency and amplitude. Indeed, the precise definitions of these parameters depend upon the ETG, and hence we make use of these definitions in order to map the burst triggers from one channel to the other.

4.1. Mapping the burst triggers

The burst detection algorithm called HACR [19, 20] is used to generate the burst triggers. HACR makes a time-frequency map of the data and identifies time-frequency pixels containing excess power which are statistically unlikely to be associated with the underlying noise. HACR then proceeds to cluster the neighboring pixels containing excess power to form an 'event'. The central frequency and time-of-occurrence of the burst-event are estimated by a weighted averaging of the pixel coordinates. This is equivalent to the calculation of the center-of-mass of an extended object where the signal power in a pixel serves as the 'mass' term. HACR also estimates the total power contained in all the pixels belonging to a particular event, and the peak-power of the event. The square root of the total power is taken as the characteristic amplitude E_X^a of the event.

The ETG does not reproduce the complete physical properties of a burst waveform. Instead, the ETG tries to parametrize the underlying waveform using a set of quantities like the central frequency, amplitude, bandwidth, duration, etc. Considering the fact that we are mostly looking at short-lived, band-limited bursts, we approximate the power spectrum of the underlying burst waveform in channel X to a Gaussian function. For example, the power spectrum of the waveform associated
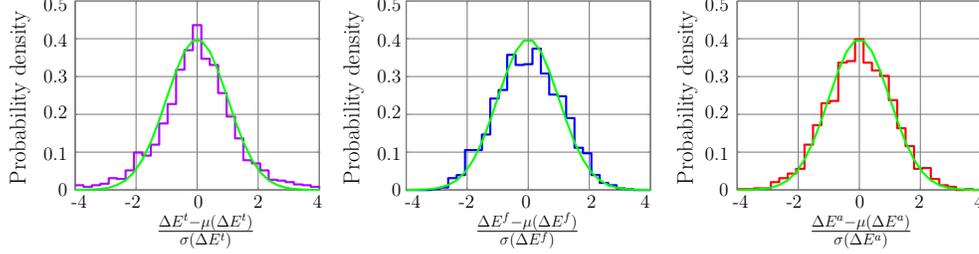
Figure 5. Distribution of HACR errors (after subtracting the mean and normalizing by the standard deviation) in estimating the parameters of the injected sine-Gaussian waveforms. Also plotted is the probability density of Normal distribution with mean 0 and variance 1.

with a trigger $\mathbf{E}_X$ is approximated to a Gaussian function $G(f)$ such that

$$\int_{f_1}^{f_2} G(f)\,\mathrm{d}f = \left(E_X^a\right)^2, \tag{13}$$

where the limits of integration are defined by bandwidth E_X^b of the burst, i.e. $f_1 = E_X^f - E_X^b/2$ and $f_2 = E_X^f + E_X^b/2$. Since the peak-power of the burst is also estimated by the ETG, the 'spread' of the Gaussian function can be calculated by solving Eq.(13). The power spectrum is 'deformed' by the transfer function $T_{XH}(f)$ when the glitch makes its way to channel H; this we denote by

$$\hat{G}(f) = G(f)\,|T_{XH}(f)|^2. \tag{14}$$

Given the transfer function $T_{XH}(f)$, the burst triggers in channel X can be mapped to channel H in the following way:

$$E_X^{a\,\prime} = \left[\int_{f_1}^{f_2} \hat{G}(f)\,\mathrm{d}f\right]^{1/2}, \tag{15}$$

$$E_X^{t\,\prime} = E_X^t + \frac{\int_{f_1}^{f_2} \hat{G}(f)\,\lambda(f)\,\mathrm{d}f}{\int_{f_1}^{f_2} \hat{G}(f)\,\mathrm{d}f}, \tag{16}$$

$$E_X^{f\,\prime} = \frac{\int_{f_1}^{f_2} \hat{G}(f)\,f\,\mathrm{d}f}{\int_{f_1}^{f_2} \hat{G}(f)\,\mathrm{d}f}. \tag{17}$$

In the above expression, $\lambda(f)$ is the frequency-normalized phase-delay (time-lag) of the transfer function $T_{XH}(f)$. i.e,

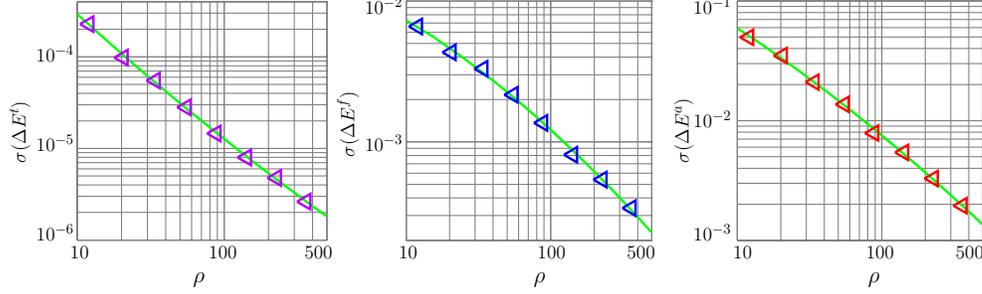$$\lambda(f) = \frac{1}{2\pi f}\,\phi\big(T_{XH}(f)\big). \tag{18}$$

where $\phi(.)$ denotes the phase of a complex quantity.

4.2. Identifying consistent events

In order to veto a trigger, $\mathbf{E}_H$, in channel H, we check whether any of the 'mapped' triggers ($\mathbf{E}'_X$) from channel X, are 'sufficiently close' to it. To be explicit, we define a vector, $\mathbf{w}$, connecting the two points in the parameter space of H triggers,

$$\mathbf{w} \equiv \mathbf{E}_H - \mathbf{E}'_X, \tag{19}$$

Figure 6. Standard deviation of the distribution of the HACR errors (in estimating the parameters of the injected sine-Gaussian waveforms) plotted as a function of the SNR of the triggers. Also shown are the polynomial fits to the data.

and require that it has a sufficiently small 'length'. This length is assigned to the vector by calculating the fractional volume enclosed by a three-dimensional Gaussian envelope of width $\sigma(\mathbf{w})$. This is explained below.

Let $\Delta \mathbf{E}$ denote the errors in the ETG in the estimation of parameters associated with the event $\mathbf{E}$. In the absence of any systematic biases, the errors $\Delta \mathbf{E}$ can be assumed to be drawn from multivariate Normal distributions of zero mean and standard deviation $\sigma(\Delta \mathbf{E})$, where the standard deviation is an exponentially decreasing function of the SNR. $\sigma(\Delta \mathbf{E})$ can be estimated by injecting known waveforms in to the data and comparing the trigger-parameters estimated by the ETG to the actual parameters of the injected waveforms.

Once the errors $\Delta \mathbf{E}_X$ associated with $\mathbf{E}_X$ are estimated, they can be mapped to the space of H triggers using Eq.(15-17) by a linear approximation of the error propagation [21]. Then the components of $\mathbf{w}$ will be distributed according to Normal distributions of zero mean and the following variance:

$$\sigma^2(\mathbf{w}) = \sigma^2(\Delta \mathbf{E}_\mathrm{H}) + \sigma^2\big(\Delta \mathbf{E}'_\mathrm{X}\big), \tag{20}$$

where $\Delta \mathbf{E}'_\mathrm{X}$ denotes the errors $\Delta \mathbf{E}_\mathrm{X}$, mapped to the space of H triggers. Thus the joint probability density of the vector $\mathbf{w}$ comprising of the three random variables (w^a, w^f, w^t) is given by the three-dimensional Gaussian function

$$f(\mathbf{w}) = \frac{1}{(2\pi)^{3/2}\,\sigma(w^f)\,\sigma(w^a)\,\sigma(w^t)} \exp\left(-\frac{1}{2}\mathbf{w}^\mathrm{T}\,\mathsf{C}^{-1}\,\mathbf{w}\right), \tag{21}$$

where $\mathbf{w}^\mathrm{T}$ denotes the transpose of $\mathbf{w}$. Assuming that the errors are uncorrelated, we write the covariance matrix C as,
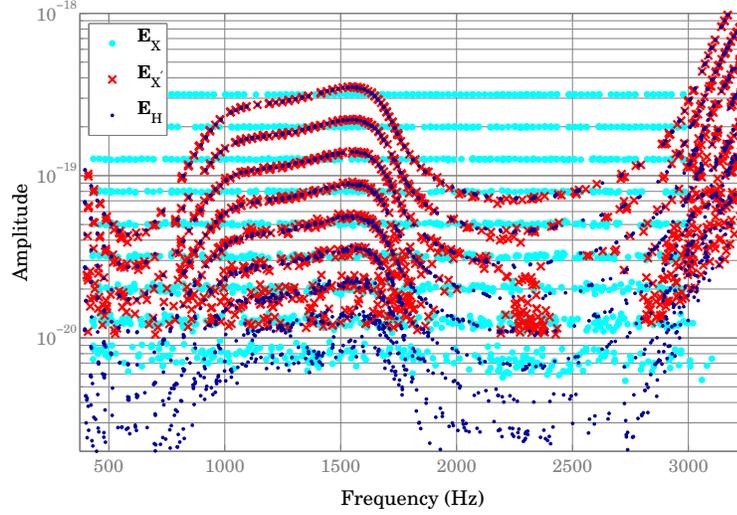
$$\mathsf{C} = \begin{bmatrix} \sigma^2(w^f) & 0 & 0 \\ 0 & \sigma^2(w^a) & 0 \\ 0 & 0 & \sigma^2(w^t) \end{bmatrix}. \tag{22}$$

This enables us to set a threshold for $\mathbf{w}$ for vetoing an event $\mathbf{E}_\mathrm{H}$. In order to veto an event, we require that

$$|\mathbf{w}| \leq \boldsymbol{\tau}. \tag{23}$$

The components (τ^a, τ^t, τ^f) of the 'threshold vector' $\boldsymbol{\tau}$ are related to the rejection probability ψ by

$$\psi = 8 \int_0^{\tau^f} \int_0^{\tau^a} \int_0^{\tau^t} f(\mathbf{w})\,\mathrm{d}w^f\,\mathrm{d}w^a\,\mathrm{d}w^t. \tag{24}$$

**Figure 7.** The RSS amplitude, E^a, of the burst-events plotted against the central frequency, E^f. Shown in the Figure are three population of events: events in channel X ($\mathbf{E}_X$); channel X events mapped to channel H ($\mathbf{E}'_X$); and events in channel H ($\mathbf{E}_H$).

It can be seen that, by choosing a particular threshold vector $\boldsymbol{\tau}$, we are defining a consistency volume around each burst trigger in channel H. If one of the mapped triggers from channel X falls in to this volume, we veto the H trigger. This is schematically illustrated in Figure 4.

4.3. Software injections

In order to estimate the variance of the distribution of HACR errors in estimating the parameters of the waveform, sine-Gaussian waveforms are injected into white noise and the HACR ETG is run over the data. The parameters estimated by the ETG are compared to the injected parameters in order to calculate the errors in the parameter-estimation. Distributions of the errors (after subtracting the mean and normalizing by the standard deviation) are plotted in Figure 5, along with the probability density of the Normal distribution with mean 0 and variance 1. The standard deviation of the errors in the estimation of different parameters are plotted as a function of the SNR of the triggers in Figure 6. It can be seen that, to a very good approximation, the standard deviation is an exponentially decreasing function of the SNR. The eight data points in the plots in Figure 6 correspond to eight different values of the RSS amplitude used for the injections. We fit the data with a simple polynomial fit and take it as the functional form of the standard deviation.

We simulate two populations of bursts in channel X and H, as described in Section 3.1. The two data streams are processed by HACR and two sets of triggers $\{\mathbf{E}_X\}$ and $\{\mathbf{E}_H\}$ are generated. The X triggers are mapped to channel H using the transfer function from X to H. Figure 7 shows the characteristic amplitude E^a of the three population of triggers ($\mathbf{E}_X, \mathbf{E}'_X$ and $\mathbf{E}_H$) plotted against the central frequency E^f. The injected events in channel X span 9 different amplitudes. The $\mathbf{E}'_X$ triggers
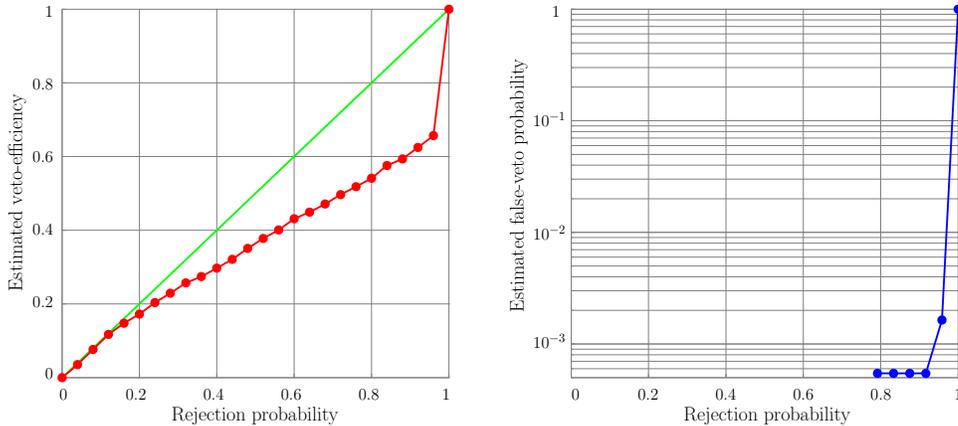
Figure 8. [*Left*]: Estimated veto efficiency plotted against the rejection probability. [*Right*]: Estimated false-veto probability plotted against the rejection probability.

and $\mathbf{E}_\mathrm{H}$ triggers can be seen to fall nicely in to the shape of the transfer function.

The veto analysis is repeated with different thresholds. The estimated veto efficiency is plotted against the rejection probability corresponding to the chosen thresholds in Figure 8. Although the estimated rejection efficiency roughly agrees with the predicted rejection probability, the effect of relying on a number of assumptions can be immediately seen. The main source of error in the analysis comes from the inaccurate parametrization of the errors in ETG in the parameter-estimation of the burst waveforms. This can be different for different ETGs.

As described in Section 3.1, we also estimate the false-veto probability by injecting sine-Gaussian waveforms with random parameters in to the two data streams and preforming the veto analysis. The estimated false-veto probability is plotted in Figure 8 (right) as a function of the rejection probability. This exercise suggests that a veto efficiency of $\sim 70\%$ can be achieved at the cost of a false-veto probability $\sim 1\%$.

5. Summary and outlook

In this paper we have formulated and demonstrated a strategy to veto spurious noise transients that appear in the output of interferometric GW detectors. This method is novel in the sense that it makes use of the measured coupling between an instrumental sub-system and the detector output in order to veto a spurious trigger. The basic idea is that the noise recorded in an instrumental channel X can be mapped in to the detector output (channel H) using the transfer function from X to H. This enables us to project the noise at the detector output in to two orthogonal directions – along, and orthogonal to, the mapped noise from channel X. If a non-stationarity in H is originated from channel X, it leaves the statistics of the component of H orthogonal to X unchanged. This can be verified by a statistical hypothesis testing. We have also proposed a less-rigorous, but computationally inexpensive alternative to the above method. In this method, the parameters of the triggers in channel X are compared to the parameters of the triggers in channel H to see whether a trigger in channel X

can explain a trigger in channel H.

Work is ongoing to incorporate the veto in the online data characterization pipeline of the GEO 600 detector [22]. So far, we have not explored the effect of the errors in measuring the transfer function. This certainly needs to be considered when the veto is applied to the actual data characterization/analysis pipeline. We leave that as future work. Also, the assumption that the transfer function is time-invariant is also not strictly true. Transfer functions in actual detectors can vary in time. This issue can be addressed by making repeated measurements of the transfer function, and tracking its evolution by continuously injecting and measuring spectral lines at certain frequencies. This is described in [16] and is already being practiced in GEO 600.

It may be noted that the 'trigger mapping' veto needs to make certain assumptions about the power spectrum of the glitch in channel X. The assumption that we made in the paper, that the power spectrum can be approximated by a Gaussian function, should be verified against real-life glitches. It might also be possible to make assumptions which are closer to the reality, using better parametrization of the underlying waveforms.

The results of the two veto methods presented in this paper may not be compared directly. The very choice of sine-Gaussian waveforms for the software injections especially favour the trigger mapping method, as they satisfy the assumption about the power spectrum of the burst waveforms that we used in the analysis. Yet, the results show that the 'noise projection' method performs better. It may be noted that the trigger mapping method also depends on the accuracy of the parameter-estimation of the ETG while the 'noise projection' veto relies only on the accuracy with which the transfer function is known.

Acknowledgments

[1] *Status of the LIGO detectors*, D Sigg (for the LIGO Scientific Collaboration), , Class. Quantum Grav. **23** (2006) S51-S56.
[2] *The status of Virgo*, F Acernese *et al* , Class. Quantum Grav. **23** (2006) S63-S69.
[3] *Status of the GEO 600 detector*, H Lück *et al* , Class. Quantum Grav. **23** (2006) S71-S78.
[4] *Current status of the TAMA300 gravitational-wave detector*, Masaki Ando and the TAMA Collaboration, Class. Quantum Grav. **22** No 18 (21 September 2005) S881.
[5] *Status report on the EXPLORER and NAUTILUS detectors and the present science run*, P Astone *et al* , Class. Quantum Grav. **23** (2006) S57-S62.
[6] *Status report and near future prospects for the gravitational wave detector AURIGA*, J-P Zendri *et al* , Class. Quantum Grav. **19** No 7 (7 April 2002) 1925-1933.
[7] http://sam.phys.lsu.edu/
[8] *One-armed Spiral Instability in a Low T/|W| Postbounce Supernova Core*, C D Ott, S Ou, J E Tohline and A Burrows, Astrophys. J. **625** (2005) L119-L122; *General Relativistic Binary Merger Simulations and Short Gamma Ray Bursts*, J A Faber, T W Baumgarte, S L Shapiro and K Taniguchi, Astrophys. J. **641** (2006) L93-L96; *Gravitational wave extraction from an inspiraling configuration of merging black holes*, J G Baker, J Centrella, D Choi, M Koppitz and J van Meter, Phys. Rev. Lett. **96** (2006) 111102; *Accurate Evolutions of Orbiting Black-Hole Binaries Without Excision*, M Campanelli, C O Lousto, P Marronetti and Y Zlochower, Phys. Rev. Lett. **96** (2006) 111101; *Accurate Evolution of Orbiting Binary Black Holes*, P Diener, F Herrmann, D Pollney, E Schnetter, E Seidel, R Takahashi, J Thornburg and J Ventrella, Phys. Rev. Lett. **96** (2006) 121101; *Gravitational-Wave Emission from Rotating*

Gravitational Collapse in three Dimensions, L Baiotti, I Hawke, L Rezzolla and E Schnetter, Phys. Rev. Lett. **94** (2005) 131101.

[9] *Excess power statistic for detection of burst sources of gravitational radiation*, W G Anderson, P R Brady, J D E Creighton and É É Flanagan, Phys. Rev. D **63**, 042003 (2001).

[10] *Time-frequency detection algorithm for gravitational wave bursts*, J Sylvestre, Phys. Rev. D **66**, 102004 (2002).

[11] *A wavelet method for detection of gravitational wave bursts*, S Klimenko and G Mitselmakher, Class. Quantum Grav. **21** No 20 (21 October 2004) S1819-S1830.

[12] *PQMon: a powerful veto for burst events*, K Kötter, I S Heng, M Hewitson, K A Strain, G Woan and H Ward Class. Quantum Grav. **20** No 17 (7 September 2003) S895-S902.

[13] *Gravitational wave burst vetoes in the LIGO S2 and S3 data analyses*, A Di Credico (for the LIGO Scientific Collaboration), Class. Quantum Grav. **22** No 18 (21 September 2005) S1051-S1058.

[14] *Using the null-stream of GEO 600 to veto transient events in the detector output*, M Hewitson and P Ajith, Class. Quantum Grav. **22** No 22 (21 November 2005) 4903-4912.

[15] *The scientist and engineer's guide to digital signal processing*, S W Smith, Second ed., California Technical Publishing (1999); Online edition at `http://www.dspguide.com`.

[16] *Linear projection of technical noise for interferometric gravitational-wave detectors*, J R Smith, P Ajith, H Grote, M Hewitson, S Hild, H Lück, K A Strain, B Willke, J Hough and K Danzmann, Class. Quantum Grav. **23** No 2 (21 January 2006) 527-537.

[17] *Mathematical methods for physicists*, G B Arfken and H J Weber, Fifth ed., Academic Press (2001).

[18] *The probability density of spectral estimates based on modified periodogram averages*, P E Johnson and D G Long, IEEE Trans. on Signal Processing **47**, 1255 (1999).

[19] *First steps towards characterizing the hierarchical algorithm for curves and ridges pipeline*, I S Heng, R Balasubramanian, B S Sathyaprakash and B F Schutz, Class. Quantum Grav. **21** No 5 (7 March 2004) S821-S826.

[20] *Results from the first burst hardware injections performed on GEO 600*, R Balasubramanian, H Grote, I S Heng, M Hewitson, H Lück, J R Smith, K A Strain, H Ward and B Willke, Class. Quantum Grav. **22** No 14 (21 July 2005), 3015-3028.

[21] *Data reduction and error analysis for the physical sciences*, P R Bevington and D K Robinson, Third ed., Mc Graw-Hill (2003).

[22] GEO Summary Reports: `http://www.geo600.uni-hannover.de/georeports`.